MINERAL IDENTIFICATION USING GER-II DATA ACQUIRED FROM MAKHTESH RAMON / NEGEV, ISRAEL

H. Kaufmann and W. Weisbrich

Department of Photogrammetry and Remote Sensing, University of Karlsruhe, FRG

M. Beyth, Y. Bartov and A. Itamar

Geological Survey of Israel, Jerusalem, Israel E. Mazor The Weizmann Institute of Science, Rehovot, Israel

S. Ronen and U. Kafri

Institute for Petroleum Research and Geophysics, Holon, Israel

Abstract

During the summer of 1989 the Geophysical Environmental Research Corp. (GER) aircraft scanner was flown in Negev highlands in Israel. Recorded data have been evaluated with regard to system requirements and their applicability for exploration purposes. They proved to be very successful for identification of minerals and rocks such as dolomite and limestone, as well as several kaolinite, bauxite and alunite bearing strata. Different, hydrothermally altered areas of the Shen Ramon could be separated and mapped using image processing techniques. However, only one zone could be identified by extracted pixel spectra. Since nominal band width and band centering comply with the nominal system parameters of the SWIR-2 module, the signal to noise ratio of about 20:1 at 0.5 albedo is far too low to detect and identify small portions of indicative minerals in a low albedo environment. Random noise simulations confirm that a SNR of at least 100:1 is required to identify indicative alteration minerals at quantities of about 5% at 0.3 albedo at a spectral resolution of 16.22 nm in the SWIR range.

1. INTRODUCTION

In connection with ESA's European flight campaign during June/July of 1989, the GER-II aircraft system was flown in Israel, where data of several different target areas were acquired. One test-site, located in the Negev, the Makhtesh Ramon, is a deeply eroded structure characterized by a high variety of Mesozoic formations. In the Makhtesh there are several quarries mined for gypsum, kaolinite and bauxite, as well as a syenitic stock that is divided into several blocks of different hydrothermally altered zones. The scope of this paper is to present preliminary results concerning data quality and evaluation of data in comparison with field derived spectra and analyses.

2. SYSTEM DESIGN

During the flight campaign on 9.7.89, the system was mounted into a Piper Aztec of the GER-Corp. New York. In the Makhtesh Ramon area, three lines were flown at an altitude of 15,000 feet above sea level (asl) and one in 5,000 feet asl. Data were recorded in 16-bit modus. Each cross-track consisted of 512 pixels. The GIFOV for the high altitude flights resulted in about 13.44 m x 13.44 m at nadir. System parameters for the visible and near infrared (VNIR) as well as for the two shortwave infrared (SWIR) modules, including number of bands, band widths, band centering and signal to noise ratios (SNR) are shown synoptically in Fig. 1. Wavelengths and calibrations file are represented in Table 1.

TABLE 1

WAVELENGTHS AND CALIBRATIONS FILE FOR THE MAKHTESH RAMON TEST- SITE.

(Source: Lehmann *et al.*, 1990, first release)

VNIR				SWIR			
channel	center wavelength [nm]	center wavenumber [cm^{-1}]	calibration file [mWcm^{-2}sr^{-1}µm^{-1}]	channel	center wavelength [nm]	center wavenumber [cm^{-1}]	calibration file [mWcm^{-2}sr^{-1}µm^{-1}]
1	477	20964	0.0539	32	1440	---	---
2	489	20450	0.0584	33	1560	6410	8.54 E-4
3	502	19920	0.0562	34	1680	5952	1.08 E-3
4	514	19455	0.0474	35	1800	5555	2.10 E-4
5	526	19011	0.0429	36	2005	4988	3.27 E-4
6	539	18553	0.0417	37	2022	4946	6.27 E-4
7	551	18149	0.0342	38	2038	4907	6.51 E-4
8	564	17730	0.0426	39	2054	4869	4.86 E-4
9	576	17361	0.0395	40	2070	4831	4.84 E-4
10	588	17007	0.0386	41	2087	4792	6.12 E-4
11	601	16639	0.0359	42	2103	4755	5.77 E-4
12	613	16313	0.0378	43	2119	4719	5.63 E-4
13	625	16000	0.0343	44	2135	4684	6.01 E-4
14	638	15674	0.0318	45	2151	4649	5.48 E-4
15	650	15385	0.0305	46	2168	4613	5.83 E-4
16	662	15106	0.0291	47	2184	4579	5.61 E-4
17	675	14815	0.0301	48	2200	4545	5.48 E-4
18	687	14556	0.0226	49	2216	4513	6.30 E-4
19	699	14306	0.0274	50	2232	4480	6.55 E-4
20	712	14045	0.0252	51	2249	4446	6.14 E-4
21	724	13812	0.0236	52	2265	4415	6.30 E-4
22	736	13587	0.0240	53	2281	4384	6.22 E-4
23	749	13351	0.0257	54	2297	4354	5.70 E-4
24	761	13141	0.0250	55	2314	4322	5.36 E-4
25	774	12920	0.0234	56	2330	4292	5.14 E-4
26	786	12723	0.0227	57	2346	4263	5.96 E-4
27	798	12531	0.0143	58	2362	4234	7.21 E-4
28	811	---	---	59	2378	4205	6.47 E-4
29	823	12151	0.0124	60	2395	4175	6.70 E-4
30	835	11976	0.0184	61	2411	4148	6.88 E-4
31	848	11792	0.0165	62	2427	4120	8.02 E-4
				63	2443	4093	7.46 E-4

3. DATA QUALITY AND CALIBRATION ACCURACY

Table 1 shows the nominal and approximative calculated values for the Makhtesh Ramon flight lines. A decrease of the SNR for the SWIR-2 module by a factor of about 20 and for the VNIR module by a factor of about 200 could be observed. Furthermore, the spectral resolution of the VNIR module turned out to be broadened by a factor of three to four.

• Wave-bands:	*63 with selectable wavelength*
• Dynamic range:	*16 bits radiometrically calibrated*
• Signal-to-noise: (0.5 Albedo)	*VNIR – range to 5000 [10–45]* *SWIR – range to 500 [5–35]*
• IFOV:	*selectable 2.5 to 4.6 mRad (3.3)*
• Pixels per scan:	*selectable (512) to 1024*
• Scan speed:	*selectable 1 to 50 scans per sec.*
• Current design:	(Makhtesh Ramon / ISRAEL)
VNIR – Module:	*477 – 848nm; 31 bands* *sampling interval: 12.37nm [~45nm]*
SWIR 1 – Module:	*1440 – 1800nm; 4 bands* *sampling interval: 120nm*
SWIR 2 – Module:	*2005 – 2443nm; 28 bands* *sampling interval: 16.22nm*

Date/GMT-Time:	*09.07.89 /10.36h*	*/10.01h*
Flight Altitude (a.s.l.):	*15000 feet*	*5000 feet*
GIFOV at 3.3 mRad:	*13.44m at Nadir*	*3.38m at N.*
Flight Direction:	*65° az.*	*65° az.*
Mean Sun Elevation:	*78.3°*	*81.1°*

Fig. 1. System parameters of the GER-II Scanner.
() = chosen variable,
[] = calculated, deviating values.

3.1 *Signal to Noise Ratio*

First of all, haze and dark-current quantities of the signal were calculated and subtracted from each band of the VNIR and SWIR-2 modules. Then, the effective SNR was approximated by ratioing the mean value of a 7 by 7 pixel matrix (defined as reflectivity) by the standard deviation (defined as noise) of rather homogeneous surface characters of different albedo. Results for a low and a medium reflectance target in the VNIR and SWIR-2 modules are illustrated in Fig. 2.

Even at targets with high albedo (not shown), the SNR in SWIR-2 never exceeded values of 50:1. However, it must be stated that current SNR values should be somewhat higher, since natural surfaces under consideration cannot show real homogenity.

3.2 *Band Centering*

Band centering was examined on the basis of known surface mineralogy only for the SWIR-2 module. Absorptions at 2168 nm (channel 46) and 2200 nm (channel 48) for a well-known kaolinite target as well as atmospheric bands at 2045 nm, 2346 nm and 2378 nm confirm the given nominal dates for this module. Values for the VNIR range will be found in Lehmann *et al.* (1990).

3.3 *Band Widths*

As a consequence of non existing inflight field measurements, effective band width was estimated by comparison of aircraft and laboratory derived spectra of one and the same surface target (kaolinite). For normalization purposes spectra were converted to radiance using the calibration file for aircraft data (Table 1) and a LOWTRAN-7 path simulation for laboratory measurements. Filtering and resampling techniques were applied to simulate different band widths (overlap) at a fixed nominal sampling interval of 16.22 nm.

The shape of the aircraft derived CO_2 band at 2060 nm is only comparable at a simulated spectral resolution of

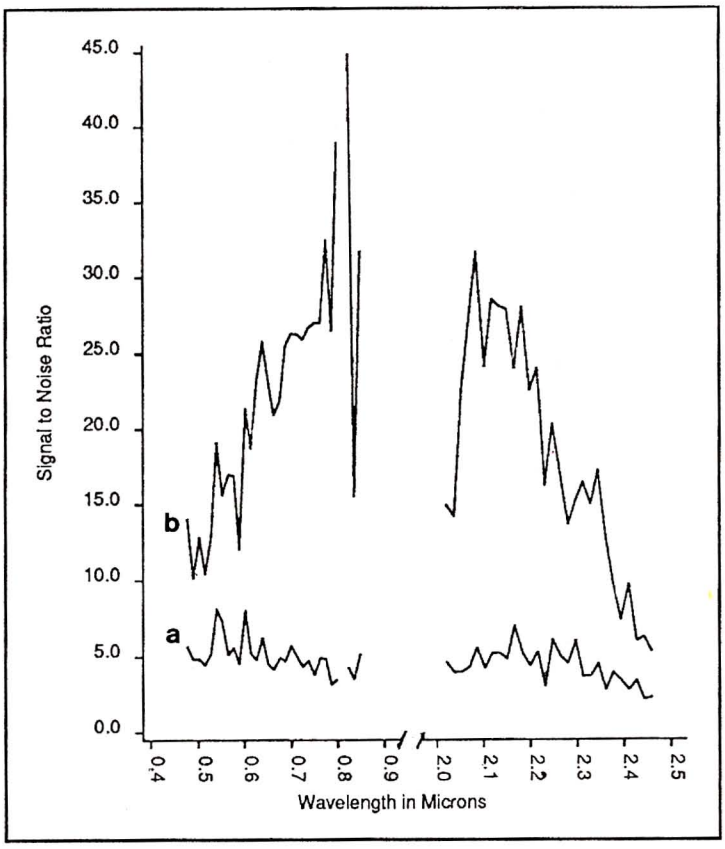

Fig. 2. SNR for a low (a) and a medium (b) reflectance target calculated for the VNIR and SWIR-2 modules.

16.22 nm (Fig. 3). At a simulative broadening of bands to 25 nm this atmospheric feature became progressively quenched. This approach confirmed that the given nominal band width should not be broadened essentially. The Al-OH absorption (approx. 2180 nm) is not displayed as a double feature. Therefore it is difficult to be analyzed comparatively in this context.

4. PROCESSING METHODS

Data processing includes several steps of pre- and post-procedures that are needed for synoptical interpretation (image optimization) and spectral-analytical data evaluation.

Preprocessing includes despiking, vertical and horizontal destripping as well as compression to 8-bits for image processing and display on screen.

To separate and enhance areas characterized by $Fe^{2+,3+}$, CO_3^{2-}, OH^- and H_2O bearing minerals, color composites of distinct bands using a decorrelation concept were generated (Kaufmann 1988).

On the visual basis of those composites, pixel spectra of interesting areas were extracted after "flat-field" and/or "log-residual" transformations (Green and Craig 1985) had been applied to the 16-bit data.

5. DATA EVALUATION

5.1 *Geological Setting*

Three major makhteshim named HaGatan, HaGadol and Ramon have been described in the Negev, of which the Makhtesh Ramon is the most extensively investigated one (Fig. 4). It shows a continuously exposed section from the Middle Triassic to the Middle Eocene (Fig. 5).

The oldest outcropping rocks, the Triassic-Gevanim formation, consists of sandstones, quartzites and marine-littoral shales. They are overlain by the Saharonian formation composed by alternating limestones, dolomites and marls. The upper Triassic is represented by marine lagoonal gypsum layers with intercalated beds and lenses of dolomite and clay and is capped by lagoonal limestones.

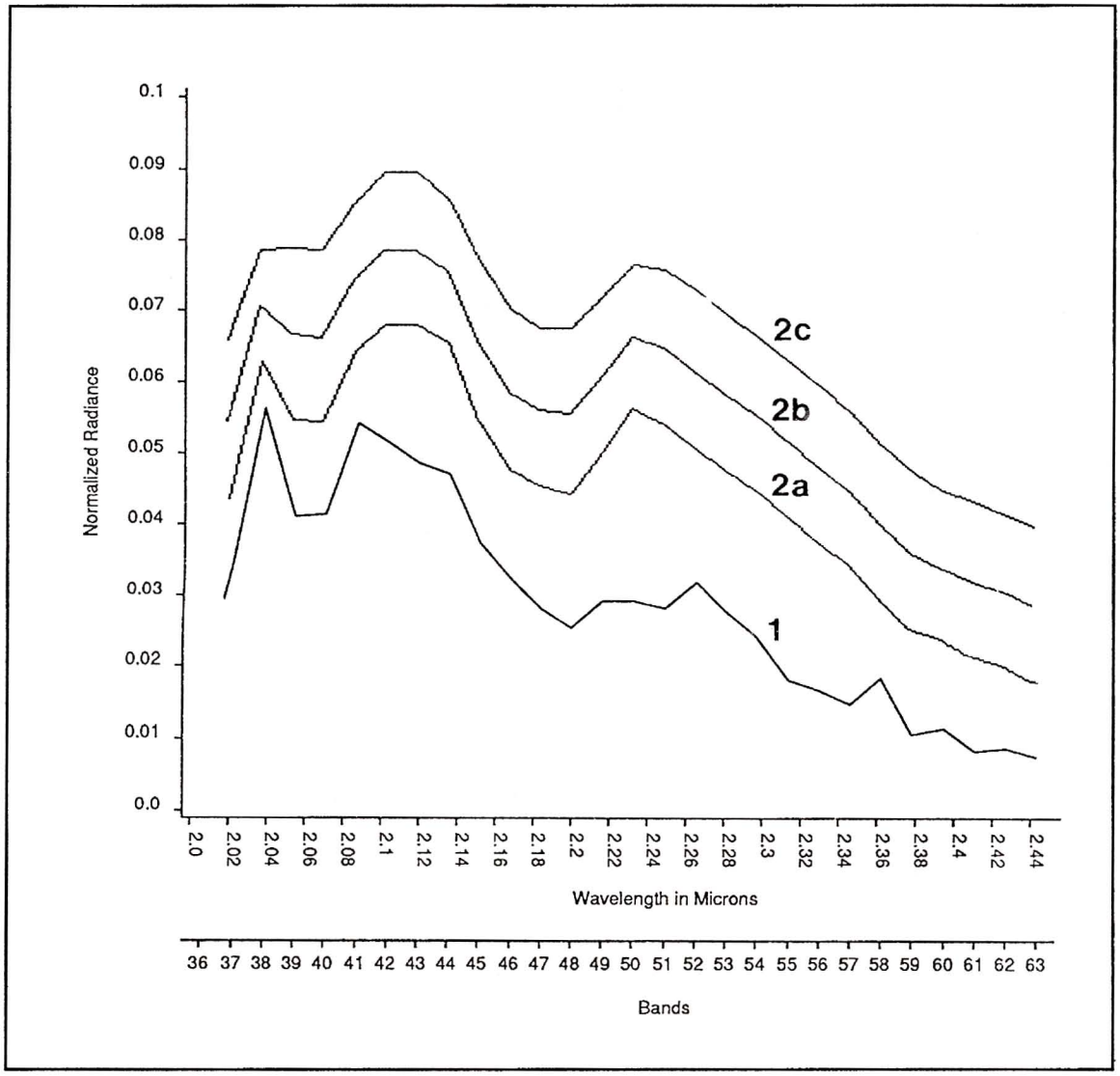

Fig. 3. Comparison of aircraft and laboratory spectra of a kaolinite target converted to normalized radiance, (1) aircraft derived spectrum; (2) laboratory data. a: filtering 16.22 nm, b: filtering 25 nm, c: filtering 35 nm. Constant resampling 16.22 nm. No noise simulations applied to laboratory data. Spectra are offset vertically for clarity.

Jurassic sediments overlie those of the Triassic inconformably. Along this plane of inconformity fossil laterites are developed that consist mainly of kaolinite and bauxite minerals (named "flint-clay"). The overlying Liassic Ardon formation is composed of multicolored shales and sandstones deposited in a shallow-water marine environment. The Early to Middle Jurassic Inmar formation is predominantly built of sandstones and lacustrine clays, followed by sandstones, dolomites and shales of the Mahaml formation.

A major inconformity separates the marine sediments of the Middle Jurassic from the continental Nubian sandstones of the Early Cretaceous (Hatira). The Cenomanian limestones and dolomites contain glauconite layers at the base and bentonite beds at the lower parts.

All rocks up to the base of the Early Cretaceous were abundantly intruded by alkaline to hyper-alkaline igneous rocks forming stocks, laccoliths, sills and dikes that are often altered by hydrothermal processes. The last magmatic activity in this area took place in Early Cretaceous and resulted in large sheet extrusions of alkaline basalts.

5.2 *Profile Har Gevanim - Nahal Ramon*

Fig. 6 shows a color composite of the central Makhtesh Ramon. Surfaces that are characterized by Fe-bearing

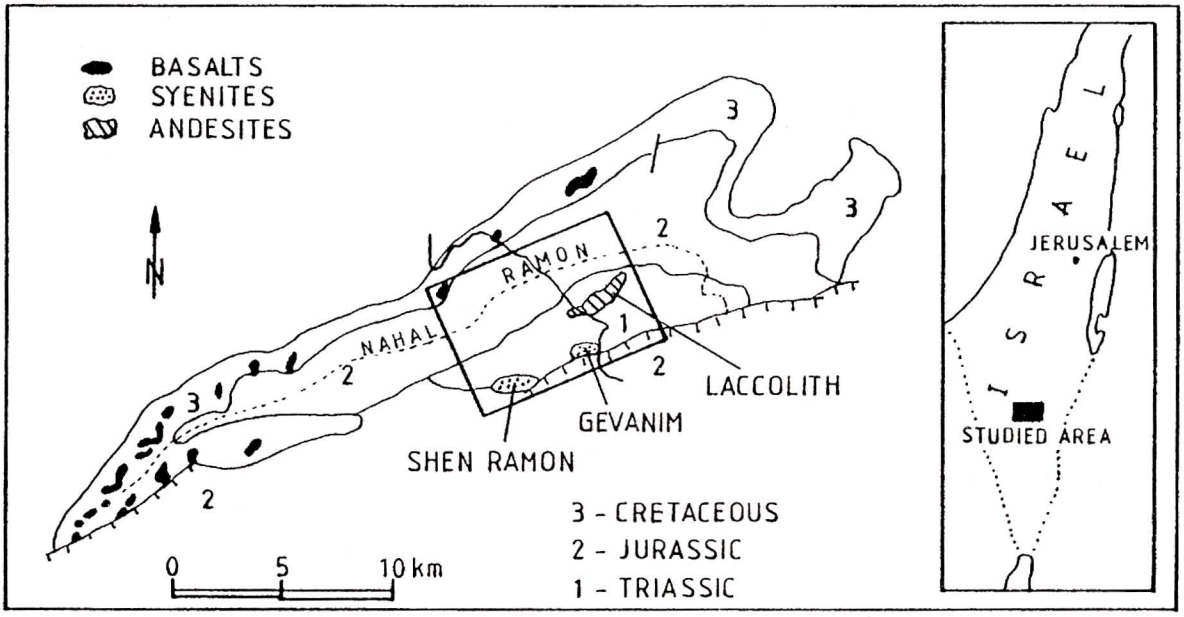

Fig. 4. Makhtesh Ramon (after Zak, 1987).

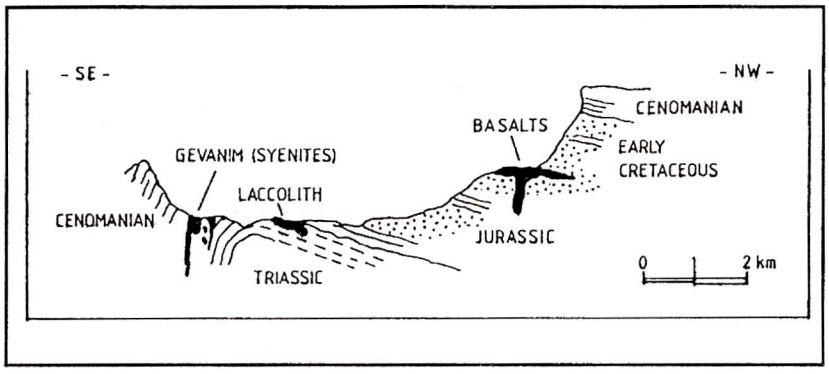

Fig. 5. Schematic cross section of the central Makhtesh Ramon (Mazor and Shoval, 1987).

minerals are enhanced in red, those marked by OH- and H_2O are enhanced in cyan colors. Areas marked by minerals containing Fe- and OH- groups are displayed in green.

A color composite of SWIR bands is shown in Fig. 7. Minerals causing 2200 nm and 2330 nm features are enhanced simultaneously due to absorptions in band 48 (kaolinite - greenish-yellow) and band 56 (carbonates - bluish-cyan). In contrast to Fig. 6, differently altered zones of the Shen Ramon and of working areas for distinct minerals can now be distinguished by their spectral behavior.

"Flat-filed" corrected spectra, together with a lithostratigraphic map are shown in Fig. 8. Despite the low SNR, most features, with the exception of gypsum, are well resolved. At the surface the gypsum is mostly altered to bassanite and anhydrite that show only weak features due to minor contents of H_2O.

5.3 *Alteration Zones of Har Shen Ramon*

Fig. 9 shows the alteration zones of the Shen Ramon (Itamar and Baer, 1986). The unaltered syenite, the so-called "roof-rock" contains quartz, feldspars and arfvedsonite. The propylitic altered rocks contain additional chlorite, epidote and are impregnated by Fe-oxides. The argillic and sericitic zones are combined within a kaolinitic zone that contains additional kaolinite, chlorite and zeolites. The rocks of the potassic zone are characterized by K-feldspar and high concentrations of Fe-oxides.

Fig. 6. Color composite of bands 1, 30 and 48, coded blue, green and red respectively. Fe-oxides appear in red due to absorptions in bands 1 and 30. Kaolinite and gypsum show cyan colors because of major absorptions in band 48. Bauxite/kaolinite are imaged green due to absorptions in the blue (1) (Fe) and red (48) (Al-OH) coded bands.

(1) syenite of Shen Ramon;
(1a) syenite of Har Gevanim;
(2) gypsum;
(3) kaolinite;
(4) bauxite/kaolinite;
(5) Wadi Ramon;
X-Y mark center line of profile of Fig. 8.

Fig. 7. Color composite of bands 48, 36 and 56, coded blue, green and red respectively. Hints to altered areas in the Shen Ramon (5-8) became visualized since solely SWIR bands are used for coding. In the composite of Fig. 6, Al-OH absorptions are masked by strong Fe- absorptions.

(1) carbonates;
(2) kaolinite;
(3) bauxite/kaolinite bed;
(3a) bauxite quarry;
(4) gypsum;
(4a) gypsum quarry;
(5) "roof- rock";
(6) propylitic zone;
(7) kaolinitic zone;
(8) potassic zone.

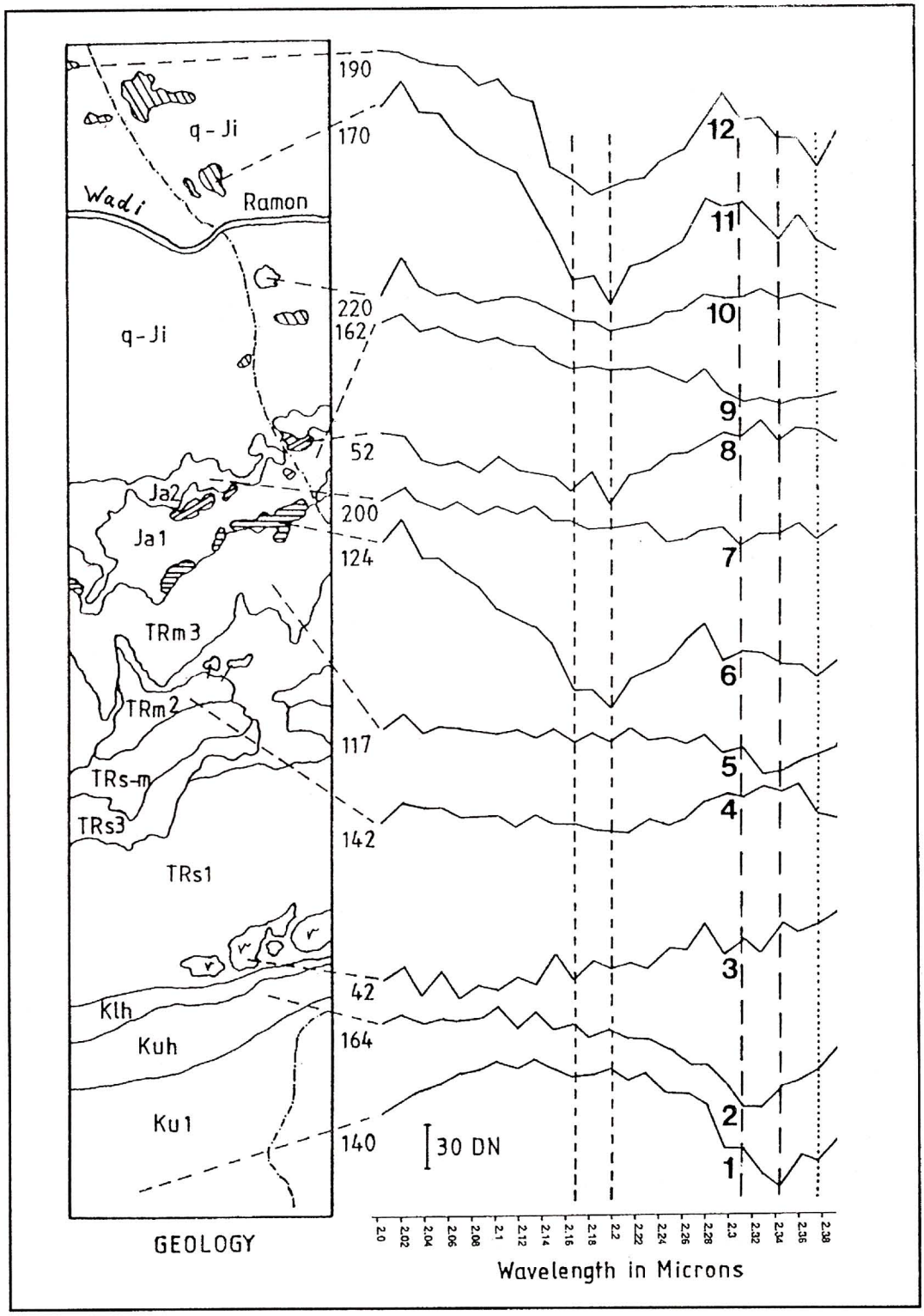

Fig. 8. Litho-stratigraphy and "flat-field" corrected pixel spectra of 3x3 matrices.
(1) limestone; (2) dolomite; (3) syenite; (4) gypsum; (5) carbonate sequences; (6) kaolinite/bauxite ("flint-clay"); (7) sandstone; (8) kaolinite ("chocolate clay"); (9) carbonatic sandstone; (10) kaolinitc sandstone; (11) kaolinite quarry; (12) kaolinite/alunite. Numbers indicate brightness of surface materials in channel 36 (2005 nm).

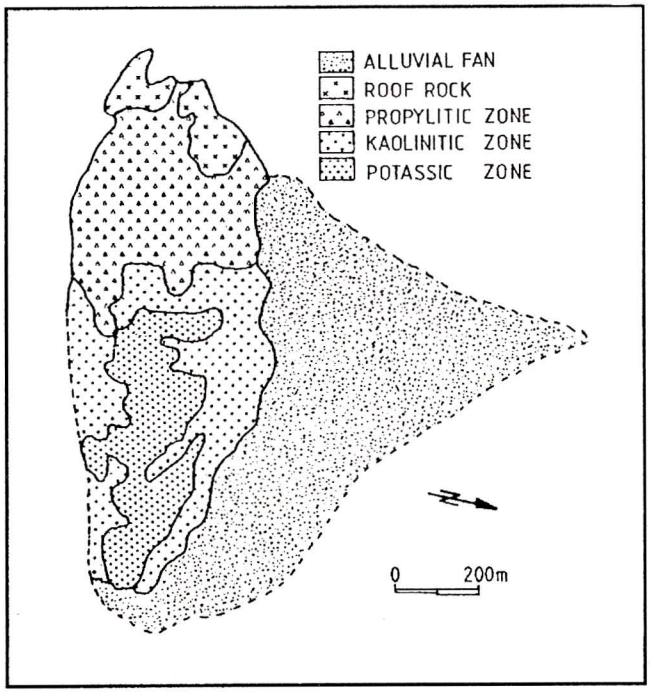

Fig. 9. Alteration zones of the Shen Ramon (after Itamar and Baer, 1986).

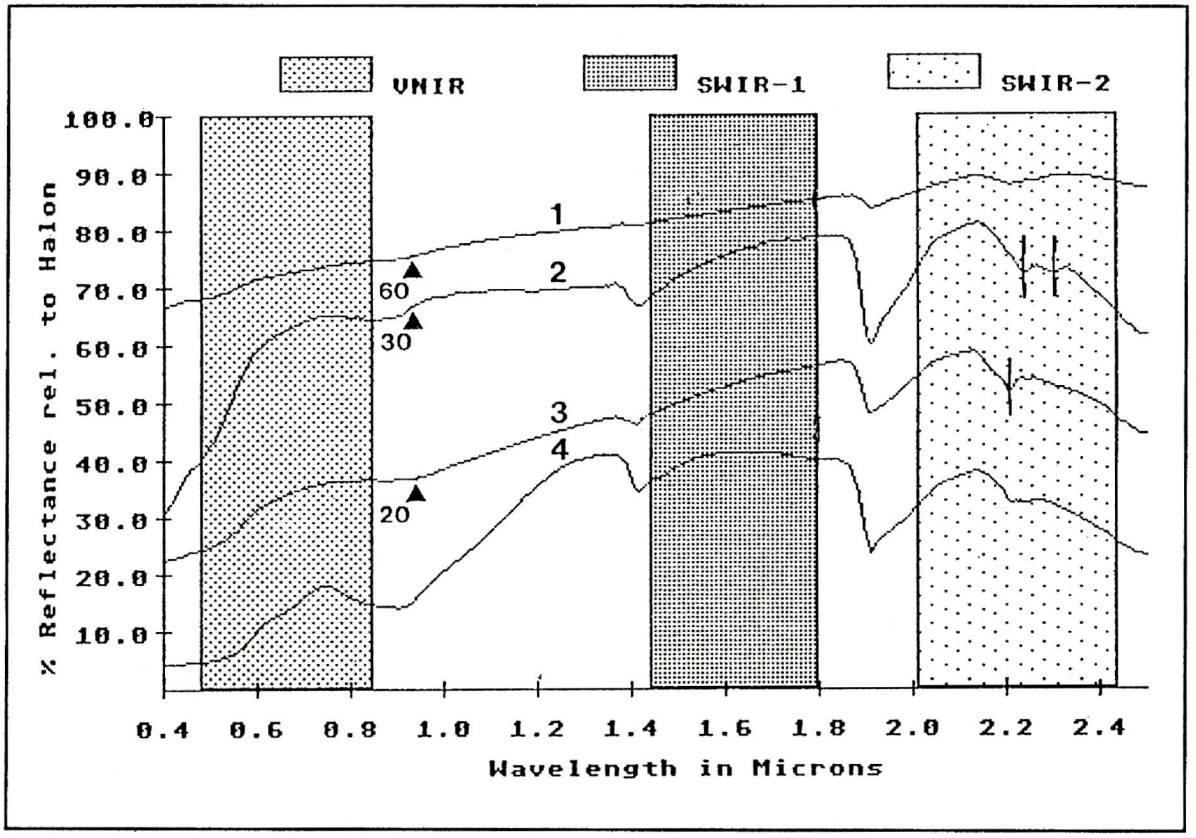

Fig. 10. Mean laboratory spectra of unaltered and altered rock samples of Shen Ramon syenites. Coverage of the GER-modules is marked. Arrows indicate vertical offset.

(1) "roof-rock"; (2) propylitic altered samples; (3) kaolinitic-altered samples; (4) potassic altered samples.

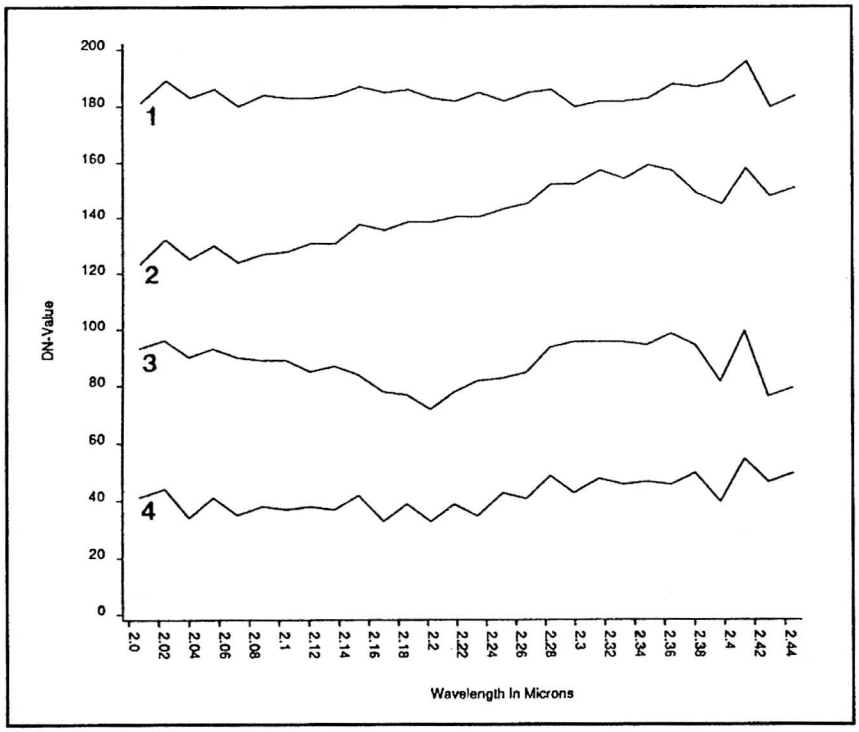

Fig. 11. Spectra of the SWIR-2 module of different alteration zones. Spectra are offset vertically for clarity.

(1) "roof-rock";
(2) propylitic zone;
(3) kaolinitic zone;
(4) potassic zone.

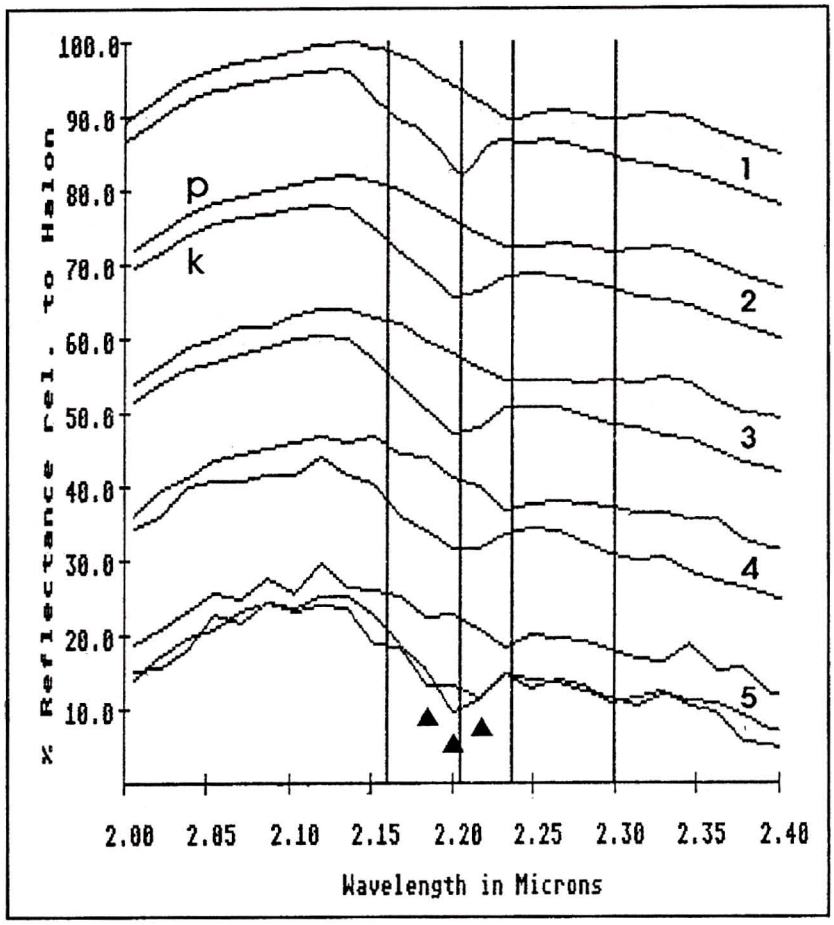

Fig. 12. SNR simulations (random generator) on SWIR-2 segment of laboratory spectra of propylitic (p) and kaolinitic (k) altered rock samples after filtering and resampling to a spectral resolution of 16.22 nm.
Shown resolution 5 nm (original 0.5 nm).

(1) original lab. curves;
(2) filtered and resampled to 16.22 nm;
(3) simulated, superimposed SNR = 80:1;
(4) simulated, superimposed SNR = 40:1;
(5) simulated, superimposed SNR = 20:1.
Arrows indicate varying features for different random noise calculations. Spectra are offset vertically for clarity.

All zones exposed can be separated (but not identified) on account of varying brightness or spectral behavior, using image processing techniques (Fig. 7). But only the green-yellowish colors, displayed by the kaolinitic zone, give clues to a Al-OH feature and associated minerals.

Mineral components of different altered rocks are only weakly expressed in the laboratory spectra (Fig. 10), on account of the opaque accessory minerals contained that cause a quenching of features (Kaufmann and Bodechtel 1989). Thus, as a consequence of a SNR of 20:1, features, with exception of an Al-OH absorption of the kaolinitic zone, are not resolved in the GER-aircraft derived spectra (Fig. 11).

6. CONCLUSIONS

The Shen Ramon alteration zones may be considered typical, low albedo surface characters, where indicative minerals have quantities of about 5vol%. Simulations shown in Fig. 12 indicate that a SNR of at least 100:1 is required to resolve the features of the propylitic and kaolinitic zone in the SWIR range at a given spectral resolution of about 16 nm. At a SNR of 80:1 a shift of weaker bands may occur. Only the strongest bands are resolved at a SNR of 40:1. The Al-OH feature of the kaolinitic zone represents the final, yet resolved absorption band at a SNR of 20:1, but it is highly related to random noise.

ACKNOWLEDGMENTS

The authors wish to thank the Ministry of Energy and Infrastructure, the Institute for Petroleum Research and Geophysics, the Geological Survey of Israel, the Weizmann Institute of Science and the Israel Chemical Industries Ltd. for providing funds to fly the GER-II- aircraft system in Israel. Special thanks to J. Dunstan.

REFERENCES

Collins, W. and Chang, S.H., 1982, "Airborne infrared mineral mapping survey of Marysville", Utah. *Proc. Multispectral Imaging Science Working Group*. Final Report, NASA-C.P.2260, III, 30-64.

Goetz, A.F.H., Vane, G., Solomon, J.E. and Rock, B.N., 1985, "Imaging spectrometry for earth remote sensing", *Science*, 228, 1147-1153.

Green, A.A. and Craig, M.D., 1985, "Analysis of aircraft spectrometer data with logarithmic residuals", *Proc. Airborne Imaging spectrometer data Analysis Workshop*. JPL-Pub.85-41, Jet Propulsion Laboratory, Pasadena, CA, 111-119.

Hunt, G.R., 1979, "Near infrared (1.2μm - 2.4μm) spectra of alteration minerals - Potential for use in Remote sensing", *Geophysics*, 44/12, 1974-1986.

Itamar, A. and Baer, G., 1986, "The implications of hydrothermal alteration and contact metamorphism associated with quartz syenite magmatism on mineralization in Makhtesh Ramon and Har Arif", Report GSI/20/86, Ministry of Energy and Infrastructure/Geological Survey, Jerusalem, Israel, 34p.

Kaufmann, H., and Bodechtel, J., 1989, "Land application of imaging spectrometry". *Proc. of Alpbach Summer School for Remote Sensing*, Alpbach, Austria, ESA SP-301, ESTEC, Noordwijk, NL, 143-150.

Kaufmann, H., 1988, "Mineral exploration along the Aqaba-Levant structure by use of TM-data. - Concepts, processing and results", *International Journal of Remote Sensing*, 10/11, 1639-1658.

Lehmann, F., Mackin, S., Richter, R., Rothfuss, H. and Waldbrodt, A., 1990, "The European imaging spectrometry campaign 1989 (EISAC) - preprocessing, processing and evaluation of the GER airborne imaging spectrometer data", *Progress Report to the European Community*, JRC, Ispra, DLR-552-14/89, DLR-Institute for Optoelectronics, Oberpfaffenhofen, FRG.

Mazor, E. and Shoval, S., 1987, "Makhtesh Ramon as a geological museum". In: Bartov, Y., (ed.) Geological field trips in the Makhtesh Ramon area. *Israel Geol. Soc. Ann. Mtg.*, Mizpr Ramon, 1-15.

Zak, I., 1987, "The structure of the Ramon arch and the Ramon line, southern Israel", *Israel Geol. Soc., Ann. Mtg.*, Mizpr Ramon, 145-147.